Microbiota-derived butyrate dynamically regulates intestinal homeostasis through regulation of actin-associated protein synaptopodin

Ruth X. Wang[a,b], J. Scott Lee[a], Eric L. Campbell[c], and Sean P. Colgan[a,1]

[a]Mucosal Inflammation Program, Department of Medicine, University of Colorado School of Medicine, University of Colorado Anschutz Medical Campus, Aurora, CO 80045; [b]Medical Scientist Training Program, University of Colorado School of Medicine, University of Colorado Anschutz Medical Campus, Aurora, CO 80045; and [c]Centre for Experimental Medicine, Queens University Belfast, Belfast BT9 7BL, Northern Ireland

Edited by Lora V. Hooper, University of Texas Southwestern Medical Center, Dallas, TX, and approved March 30, 2020 (received for review October 8, 2019)

The intestinal mucosa exists in dynamic balance with trillions of luminal microbes. Disruption of the intestinal epithelial barrier, commonly observed in mucosal inflammation and diseases such as inflammatory bowel diseases (IBDs), is often associated with dysbiosis, particularly decreases in species producing short-chain fatty acids (SCFAs), such as butyrate. It remains unclear to what extent microbiota-derived factors contribute to the overall maintenance of intestinal homeostasis. Initial studies revealed that butyrate selectively promotes epithelial barrier function and wound healing. We aimed to define the specific mechanism(s) through which butyrate contributes to these epithelial responses. Guided by an unbiased profiling approach, we identified the dominant regulation of the actin-binding protein synaptopodin (SYNPO). Extensions of this work revealed a role for SYNPO in intestinal epithelial barrier function and wound healing. SYNPO was localized to the intestinal epithelial tight junction and within F-actin stress fibers where it is critical for barrier integrity and cell motility. Butyrate, but not other SCFAs, induced SYNPO in epithelial cell lines and murine colonic enteroids through mechanisms possibly involving histone deacetylase inhibition. Moreover, depletion of the microbiota abrogated expression of SYNPO in the mouse colon, which was rescued with butyrate repletion. Studies in *Synpo*-deficient mice demonstrated exacerbated disease susceptibility and increased intestinal permeability in a dextran sulfate sodium colitis model. These findings establish a critical role for the microbiota and their products, specifically butyrate, in the regulated expression of SYNPO for intestinal homeostasis and reveal a direct mechanistic link between microbiota-derived butyrate and barrier restoration.

epithelial tight junctions | short-chain fatty acids | intestinal barrier | IBD

Intestinal epithelial cells (IECs) regulate mucosal homeostasis by compartmentalizing the host immune system (1). IECs thrive in an environment that harbors trillions of commensal microbes and multiple stimuli that are potentially inflammatory. Within the epithelial monolayer, tight junctions constitute the most apical complex linkage between adjacent cells and bear responsibility for regulating paracellular passage between the apical and basolateral membranes (2). Barrier impairment and resulting epithelial permeability contribute fundamentally to mucosal inflammation in diseases such as inflammatory bowel diseases (IBDs) by permitting an influx of luminal antigens that continually stimulate the mucosal immune system, potentially incurring intolerance to the gut microbiota (3, 4). Inflammatory insult damages the intestinal epithelium, necessitating mucosal wound healing for successful resolution. Following wounding, the surrounding polarized columnar epithelial cells depolarize and flatten to rapidly migrate into the denuded area and then repolarize to cover the wound in a process termed "epithelial restitution." Proliferation then follows to replenish the colonocyte pool, with balanced differentiation of the IECs and reestablishment of the tight junctions to restore barrier function (5, 6). Restoration of barrier function is crucial for inflammatory resolution and a return to intestinal homeostasis.

Microbial supply of butyrate, a fermentation-derived short-chain fatty acid (SCFA), is a critical component of gut homeostasis and determinant of disease resistance. The human gastrointestinal (GI) tract maintains a fine-tuned relationship with the commensal population where the microbiota aids digestion and, through anaerobic fermentation, locally synthesizes SCFAs (butyrate, propionate, acetate), reaching luminal concentrations of 130 mM (7). Butyrate is the favored energy source for colonocytes, with >95% of luminally derived butyrate absorbed and utilized within the colon, whereas propionate and acetate enter hepatic circulation (8, 9). Beyond energy provision, butyrate influences the mucosal environment through activation of SCFA-specific G protein-coupled receptors and regulation of gene expression by hypoxia-inducible factor (HIF) stabilization and histone deacetylase (HDAC) inhibition (10–13). Importantly, dysbiosis in IBD patients selectively decreases butyrate-producing microbial species, and IBD colonocytes show reduced ability to transport and utilize butyrate (14, 15). While the beneficial influences of butyrate on intestinal homeostasis cannot be underestimated (16, 17), the specific molecular targets of butyrate that impact barrier function and wound healing are not fully elucidated.

Significance

Intestinal epithelial barrier dysfunction and dysbiosis are central themes of inflammatory bowel diseases (IBDs). Initial studies revealed that the SCFA butyrate selectively promotes epithelial wound-healing responses. Using unbiased single-cell RNA sequencing approaches, we identified a cluster of actin-associated genes regulated by butyrate. Among these, we showed the selective induction of SYNPO as an intestinal tight junction protein with a central role in epithelial barrier regulation. Studies in vivo revealed that microbiota depletion abolished SYNPO expression that was rescued with butyrate. Analysis of *Synpo*-deficient mice revealed increased susceptibility to colitis and delayed resolution of disease with increased mucosal permeability. These findings highlight a fundamental contribution of the microbiota to homeostatic intestinal mucosal function through selective regulation of SYNPO.

Author contributions: R.X.W., J.S.L., and S.P.C. designed research; R.X.W. and J.S.L. performed research; E.L.C. contributed new reagents/analytic tools; R.X.W., J.S.L., and S.P.C. analyzed data; and R.X.W. and S.P.C. wrote the paper.

The authors declare no competing interest.

This article is a PNAS Direct Submission.

[1]To whom correspondence may be addressed. Email: sean.colgan@ucdenver.edu.

This article contains supporting information online at https://www.pnas.org/lookup/suppl/doi:10.1073/pnas.1917597117/-/DCSupplemental.

First published May 12, 2020.

In the present studies, we identify synaptopodin (SYNPO) as a butyrate-induced gene essential to IEC function during health and disease. SYNPO was originally described in renal podocyte foot processes and postsynaptic densities of neuronal synapses yet remained unstudied in the intestinal mucosa (18, 19). SYNPO belongs to the class of proline-rich actin-associated proteins that modulate cell shape and motility through regulating actin filament assembly, stress fiber formation, and cell–cell interactions via tight junction formation and maintenance (20–22). Here, we characterize SYNPO as a microbiota-derived butyrate-regulated intestinal epithelial tight junction protein that fine-tunes barrier integrity and promotes epithelial restitution following wounding.

Results

Butyrate Uniquely Promotes Intestinal Barrier Function and Accelerates IEC Wound Restitution. In initial studies, we defined the impact of butyrate on epithelial barrier function. To do this, transepithelial electrical resistance (TEER) as a measure of barrier function was monitored in T84 IECs grown on permeable inserts in the presence and absence of butyrate. Cells exposed to 1 mM butyrate more rapidly reached significantly higher TEER by 24 h and maintained nearly twice the magnitude of TEER at the end of 48 h compared to control cells (butyrate: 2,340 ± 118.0 Ω•cm^2; to control: 1,307 ± 126.2 Ω•cm^2, $P < 0.0001$) (Fig. 1*A* and *SI Appendix*, Table S1). Treatment with equivalent concentrations of acetate and propionate did not significantly increase barrier at 48 h compared to control (Fig. 1*B* and *SI Appendix*, Table S1). Similarly, butyrate treatment in scratch wounded T84 cells significantly accelerated the rate and increased the extent of wound closure by 75.23% compared to control cells over 38 h (butyrate: 90.35 ± 1.937%; to control: 15.12 ± 2.646%, $P < 0.0001$) (Fig. 1*C* and *SI Appendix*, Table S2). Propionate and acetate treatment influenced wound restitution significantly less compared to butyrate (Fig. 1*D* and *SI Appendix*, Table S2). Representative T84 scratch wounds fully reepithelialized with butyrate (Fig. 1*E* and Movies S1 and S2), and, within 6 h, butyrate-treated cells at the leading migratory edge showed a more elongated morphology and lamellipodia-like extensions absent in the control cells (Fig. 1*F*).

Butyrate Selectively Induces the Expression of SYNPO. Given this prominent and selective barrier and wound-healing phenotype, we extended these studies to objectively define new targets for butyrate-mediated epithelial function. In parallel, we also wondered how variable butyrate responses might be in a relatively homogenous cell population (i.e., T84 cells). For these purposes, we performed an unbiased single-cell RNA sequencing (scRNAseq) screen on T84 cells subjected to physiologically relevant concentrations of butyrate (5 mM, 8 h) compared to vehicle control. As shown in *SI Appendix*, Fig. S1, while some variability was evident in the number of reads per cell and the number of genes detected per sample, among these parameters, no statistical differences were noted among the 22 T84 cell genomes sequenced. The scRNAseq relationships were visualized with principal component analysis (PCA) (Fig. 2*A*), and permutational multivariate analysis of variance (MANOVA)/Adonis was applied to test for significant associations between measured variables and gene expression, which revealed a strong shift in butyrate-mediated changes in gene expression ($P < 0.05$). *SI Appendix*, Table S3 lists the top 100 induced and repressed genes from this screen.

From the scRNAseq, we then screened for candidate target genes that may influence barrier function and/or wound-healing responses. This analysis identified a cluster of genes with such a potential (*SI Appendix*, Table S3) that included genes whose proteins promote cell migration (CTD small phosphatase-like

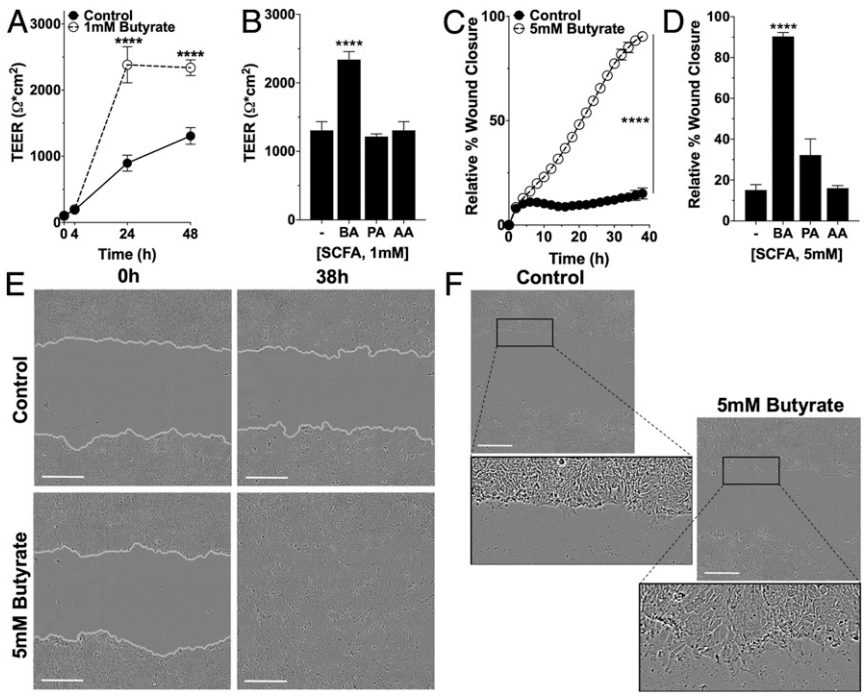

Fig. 1. Influence of SCFAs on barrier formation and wound healing. (*A*) TEER measurements over time in T84 cells on permeable inserts treated with 1 mM butyrate ($n = 6$; error bars: SEM, ****$P < 0.0001$ by two-way ANOVA, Fisher's multiple comparison). (*B*) TEER measurement at 48 h of T84 cells treated with 1 mM butyrate (BA), propionate (PA), or acetate (AA) ($n = 6$; error bars: SEM, ****$P < 0.0001$ by one-way ANOVA, Fisher's multiple comparison). (*C*) Scratch wound healing monitored over time by relative wound closure percentage in T84 cells treated with 5 mM butyrate ($n = 5$; error bars: SEM, ****$P < 0.0001$ by two-way ANOVA, Fisher's multiple comparison). (*D*) Relative wound closure percentage at 38 h of T84 cells treated with 5 mM BA, PA, or AA ($n = 5$; error bars: SEM, ****$P < 0.0001$ by 1-way ANOVA, Fisher's multiple comparison). (*E*) Live cell images of scratch wound healing (0 h, 38 h) in T84 control cells and cells treated with 5 mM butyrate (gray, cell migration/wound edge). (Scale bar: 300 μm, 10×.) (*F*) Live cell images of the migratory edge at 6 h in control and T84 cells treated with 5 mM butyrate. (Scale bar: 300 μm, 10×.)

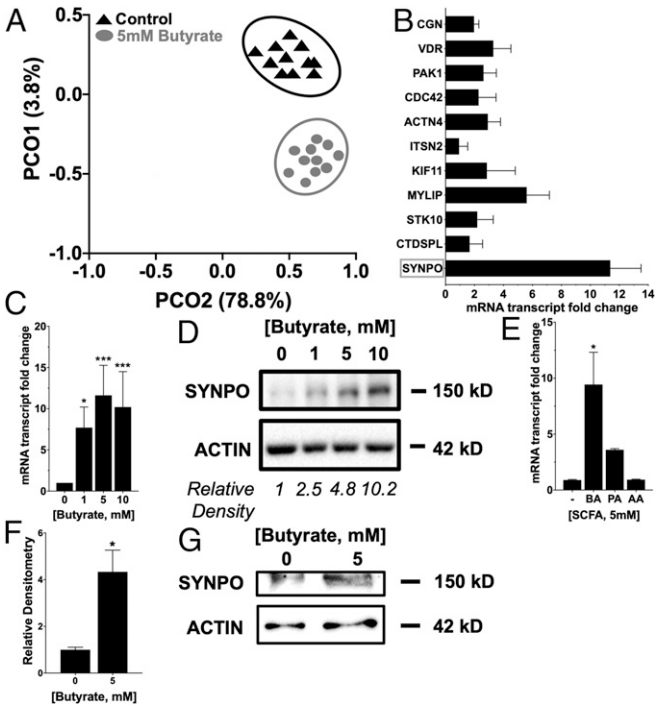

Fig. 2. Butyrate induction of genes of interest to barrier function and wound healing. (*A*) PCA plot (each point represents a cell) characterizing T84 scRNAseq data treated with or without butyrate (5 mM, 8 h) using gene expression profiling ($P < 0.05$ by permutational MANOVA/Adonis). (*B*) Induced targets of interest from scRNAseq related to wound healing and barrier function validated by qPCR in T84 cells treated with 5 mM butyrate for 6 h. (*C*) *SYNPO* mRNA expression in T84 cells treated with butyrate (0 to 10 mM) over 6 h ($n = 3$; error bars: SEM, $*P < 0.05$, $***P < 0.001$ by one-way ANOVA, Fisher's multiple comparison). (*D*) SYNPO protein expression in T84 cells treated with butyrate (0 to 10 mM) over 6 h and densitometry. (*E*) *SYNPO* mRNA expression in T84 cells treated with 5 mM butyrate (BA), propionate (PA), and acetate (AA) over 6 h ($n = 3$; error bars: SEM, $*P < 0.05$ by one-way ANOVA, Fisher's multiple comparison). (*F*) SYNPO protein expression in murine intestinal organoids/enteroids treated with 5 mM butyrate for 6 h ($n = 4$; error bars: SEM, $*P < 0.05$ by Student's *t* test). (*G*) Representative Western blot for control enteroids and enteroids treated with 5mM butyrate.

[CTDSPL], SYNPO, olfactory receptor E38 [OR7E38], serine/threonine kinase-10 [STK10])] (23–25), localize to epithelial tight junctions (cingulin [CGN], claudin-1 [CLDN1], claudin-3 [CLDN3]) (26, 27), or function in myosin/kinesin-based motor complexes (myosin regulatory light chain interacting protein [MYLIP], kinesin-11 [KIF11], intersectin-2 [ITSN2]) (28–30). This analysis suggests that butyrate-dependent regulation of the cytoskeleton may mediate barrier protection like we have recently proposed for purines (31). SYNPO was a top induced target out of the genes of interest in promoting barrier function and wound healing validated in T84 cells treated with 5 mM butyrate for 6 h (Fig. 2*B*). Treatment with butyrate at 1, 5, and 10 mM significantly induced *SYNPO* expression at the messenger RNA (mRNA) and protein level in T84 cells after 6 h, with 10 mM inducing a 10.2 ± 4.31-fold increase in mRNA ($P < 0.0001$) and a corresponding 10.2-fold protein induction compared to nontreated cells (Fig. 2 *C* and *D*). Treatment with equimolar acetate and propionate did not significantly increase *SYNPO* mRNA expression compared to nontreated cells over 6 h (Fig. 2*E*). Additionally, 5 mM butyrate treatment in murine intestinal organoids/enteroids increased SYNPO protein expression by 3.05 ± 0.669-fold ($P < 0.05$) after 6 h (Fig. 2 *F* and *G*).

Butyrate Regulates SYNPO through HDAC Inhibition. One well-established mechanism of gene regulation by butyrate is HDAC inhibition. Treatment with 300 and 500 nM trichostatin A (TSA), a potent pan-HDAC inhibitor over 6 h induced *SYNPO* mRNA by 5.99 ± 0.765-fold ($P < 0.01$) and 6.86 ± 0.883-fold ($P < 0.0001$), respectively, similar to treatment with 5 mM butyrate compared to control cells (butyrate: 8.03 ± 1.742-fold; to control: 1.00 ± 0.011-fold, $P < 0.0001$) (Fig. 3*A*). Induction of *SYNPO* mRNA with 500 nM TSA translated to a 2.1-fold increase in protein (Fig. 3*B*). *P21*, a gene known to be regulated by butyrate through HDAC inhibition (13), also showed increased mRNA with 300 and 500 nM TSA as well as with 5 mM butyrate. After a 2-h pretreatment with 10 μM C646, a histone acetyltransferase (HAT) inhibitor used essentially to stop HDAC inhibition (HDAC inhibition-inhibitor), *SYNPO* induction by butyrate was lost at the mRNA (Fig. 3*C*) and protein level (Fig. 3*D*). *P21* mRNA induction through HDAC inhibition by butyrate was similarly prevented with C646 pretreatment compared to control dimethyl sulfoxide (DMSO) pretreatment. These data suggest that histone acetylation is important to *SYNPO* transcription. When HATs are inhibited with C646 and histones are not acetylated, this then negates the influence of HDAC inhibition since histones that are not acetylated cannot be further acted upon by HDACs, and butyrate can no longer induce *SYNPO* expression. These results suggest that regulation of SYNPO by butyrate could be through HDAC inhibition.

SYNPO Localizes to the Intestinal Epithelial Tight Junction. Immunofluorescent staining was utilized in T84 cells grown on coverslips to localize SYNPO in IECs. SYNPO staining colocalized strongly with a well-known tight junction-associated protein, zonula occludens-1 (ZO-1), and demonstrated the classic chicken wire pattern correlated to the tight junction (Fig. 4*A*). Orthogonal *z* axis projection of confocal microscopy confirmed the apical localization of SYNPO and colocalization with ZO-1, as opposed to the basolateral localization of the nucleus indicated by 4′,6-diamidino-2-phenylindole (DAPI) staining (Fig. 4*B*). In mouse colonic tissue, SYNPO immunofluorescence again showed tight junction colocalization with ZO-1 (Fig. 4*C*). Colocalization analysis showed a significantly increased correlation between SYNPO and ZO-1 immunofluorescence (Pearson's correlation coefficient [PCC] = 0.71 ± 0.036, $P < 0.0001$) as compared to the correlation between SYNPO and DAPI (PCC = −0.14 ± 0.100) and ZO-1 to DAPI (PCC = −0.16 ± 0.043) (Fig. 4*D*). Secondary-only staining revealed no extraneous cellular staining (*SI Appendix*, Fig. S2*A*) but did reveal that the SYNPO antibody localized nonspecifically in mouse colonic tissue to nontight junction areas (*SI Appendix*, Fig. S2*B*). Additionally, when focusing on phalloidin-stained actin stress fibers in T84 cells, cells treated with 5 mM butyrate showed a significant increase in SYNPO levels associated with stress fibers compared to control treated cells when quantified as colocalized SYNPO and phalloidin stress fibers per region of interest (ROI) (Fig. 4 *E* and *F*).

Regulation of Barrier Formation and Wound Healing by Butyrate Requires SYNPO. To delineate the role of SYNPO in barrier function and wound restitution, knockdown (KD) of SYNPO was achieved through lentiviral transduction in T84 cells. *SYNPO* mRNA expression in the knockdown cells (SYNPO KD) was reduced by 87.67% compared to short hairpin control (SHC) ($P < 0.05$) (Fig. 5*A*), and protein was reduced by 80% (Fig. 5*B*). The SYNPO KD cells appeared morphologically distinct from the SHC cells, forming a more clustered as opposed to monolayer appearance (Fig. 5*C*). In monitoring barrier formation, the SYNPO KD cells at baseline lacked the ability to form barrier, showing a diminished rate of TEER increase and reaching a significantly lower TEER compared to SHC cells over 48 h (69.9 ± 11.23% decrease, $P < 0.0001$). Additionally, 1 mM butyrate

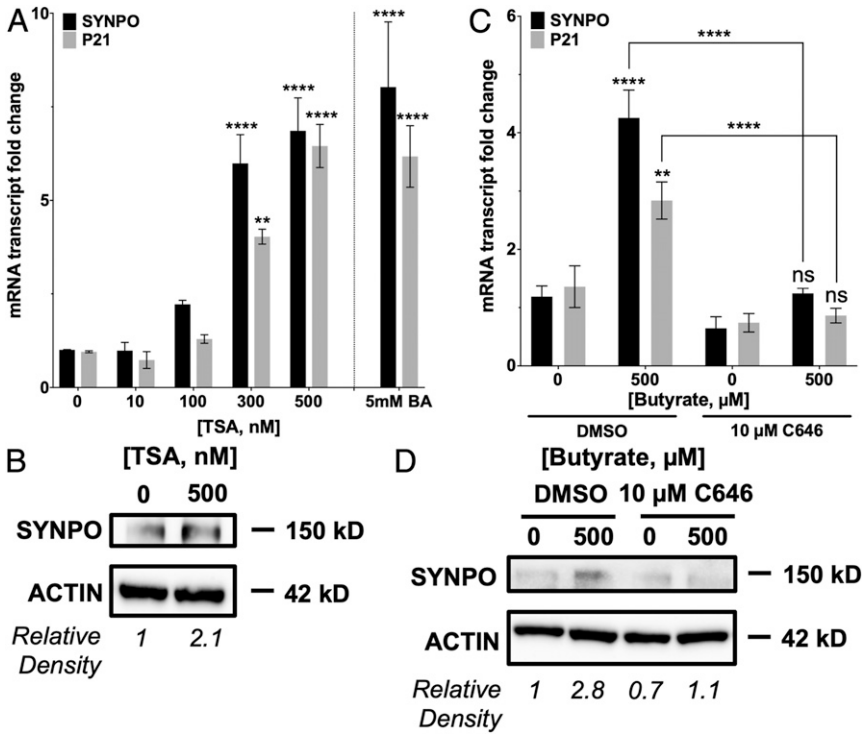

Fig. 3. Contribution of HDAC inhibition to butyrate regulation of SYNPO. (*A*) *SYNPO* and *P21* mRNA expression in T84 cells treated with HDAC inhibitor TSA (0 to 500 nM) over 6 h ($n = 3$; error bars: SEM, $^{**}P < 0.01$, $^{****}P < 0.0001$ by one-way ANOVA, Fisher's multiple comparison). (*B*) SYNPO protein expression in T84 cells treated with TSA (500 nM) over 6 h and densitometry. (*C*) *SYNPO* and *P21* mRNA expression in T84 cells pretreated with HAT inhibitor C646 (10 μM, 2 h), followed by butyrate treatment (500 μM) over 6 h ($n = 3$; error bars: SEM, $^{**}P < 0.01$, $^{****}P < 0.0001$ by two-way ANOVA, Fisher's multiple comparison). (*D*) SYNPO protein expression in T84 cells pretreated with C646 (10 μM, 2 h), followed by butyrate treatment (500 μM) over 6 h and densitometry.

treatment did not compensate the loss of barrier formation in the SYNPO KD cells and did not increase TEER compared to control-treated SYNPO KD cells at the end of 48 h (butyrate: 189.3 ± 4.98 Ω•cm^2; to control: 128.9 ± 5.82 Ω•cm^2, P = not significant [ns]). It is notable that 1 mM butyrate treatment did accelerate and promote the formation of a significantly tighter barrier in the SHC cells as expected (Fig. 5*D* and *SI Appendix*, Table S4). The relative fold change in final TEER reached due to butyrate compared to control treatment was significantly decreased in SYNPO KD (1.47 ± 0.0386-fold) versus SHC cells (3.16 ± 0.112-fold, $P < 0.0001$) (*SI Appendix*, Fig. S3*A*). To further assess barrier function, the rate of paracellular flux was determined using 3-kDa fluorescein isothiocyanate (FITC)-dextran in SYNPO KD and SHC cells treated with and without butyrate. SYNPO KD cells at baseline exhibited significantly higher permeability and increased FITC-dextran flux (SYNPO KD: 14.01 ± 0.74 [ng/μL]/h; to SHC: 1.53 ± 0.115 [ng/μL]/h, $P < 0.0001$) that persisted in SYNPO KD cells treated with 1 mM butyrate ($P < 0.0001$) (Fig. 5*E*). While butyrate treatment did not significantly decrease FITC-dextran flux in SHC cells, butyrate treatment did significantly decrease FITC-dextran flux in the SYNPO KD cells ($P < 0.0001$). However, the percentage of remaining FITC-dextran flux after butyrate treatment was significantly higher in SYNPO KD cells (59.88 ± 3.718%) compared to SHC cells (48.70 ± 1.539%, $P < 0.05$) (*SI Appendix*, Fig. S3*B*). These results suggest that, although not the sole regulator, SYNPO is still a critical component to epithelial barrier function with selective regulation by butyrate.

Similarly, the SYNPO KD cells showed a baseline deficit in the rate and magnitude of scratch wound healing compared to SHC cells (SYNPO KD: 34.51 ± 1.014%; to SHC: 48.26 ± 4.609%, $P < 0.01$). When treated with 1 mM butyrate, the SYNPO KD cells could not accelerate wound healing and did not reach a significantly different percentage of relative wound closure compared to control-treated SYNPO KD cells at the end of 38 h (butyrate: 38.14 ± 1.243%; to control: 34.51 ± 1.014%, P = ns). Similar to our results with barrier function, 1 mM butyrate exposure in SHC cells promoted wound closure compared to control treatment (Fig. 5*F* and *SI Appendix*, Table S5). The relative fold increase in wound closure due to butyrate compared to control treatment was significantly decreased in SYNPO KD (1.09 ±0.0220) versus SHC cells (1.19 ± 0.0398, $P < 0.05$) (*SI Appendix*, Fig. S3*C*). Although the fold change in wound closure is statistically significant between SHC and SYNPO KD cells, the closeness in magnitude again suggests that, while SYNPO is not the only regulator for wound healing, it is still an important player in the multifaceted promotion of epithelial barrier elicited by butyrate. Actin cytoskeletal dynamics in SYNPO KD and SHC cells were assessed by comparing the relative ratios of filamentous (F)-actin to total actin comprised of globular (G)- and F-actin. In T84 cells, treatment with 5 mM butyrate significantly increased the ratio of F-actin to total actin ($P < 0.05$). To validate the assay, treatment with 10 μM cytochalasin D, a blocker of actin polymerization and elongation of F-actin, decreased the ratio of F-actin to total actin ($P < 0.05$). In SHC cells, 5 mM butyrate similarly increased the ratio of F-actin to total actin as seen in T84 cells ($P < 0.05$). However, F-actin to total actin ratio did not increase in the SYNPO KD cells treated with 5 mM butyrate. At baseline, the SYNPO KD cells did not differ from the SHC cells in the F-actin to total actin ratio, but, in response to 5 mM butyrate treatment, the SYNPO KD cells showed a significantly lower ratio of F-actin to total actin compared to SHC cells ($P < 0.01$, Fig. 5*G*). Thus, enhanced epithelial restitution mediated by butyrate requires actin-based coupling to SYNPO.

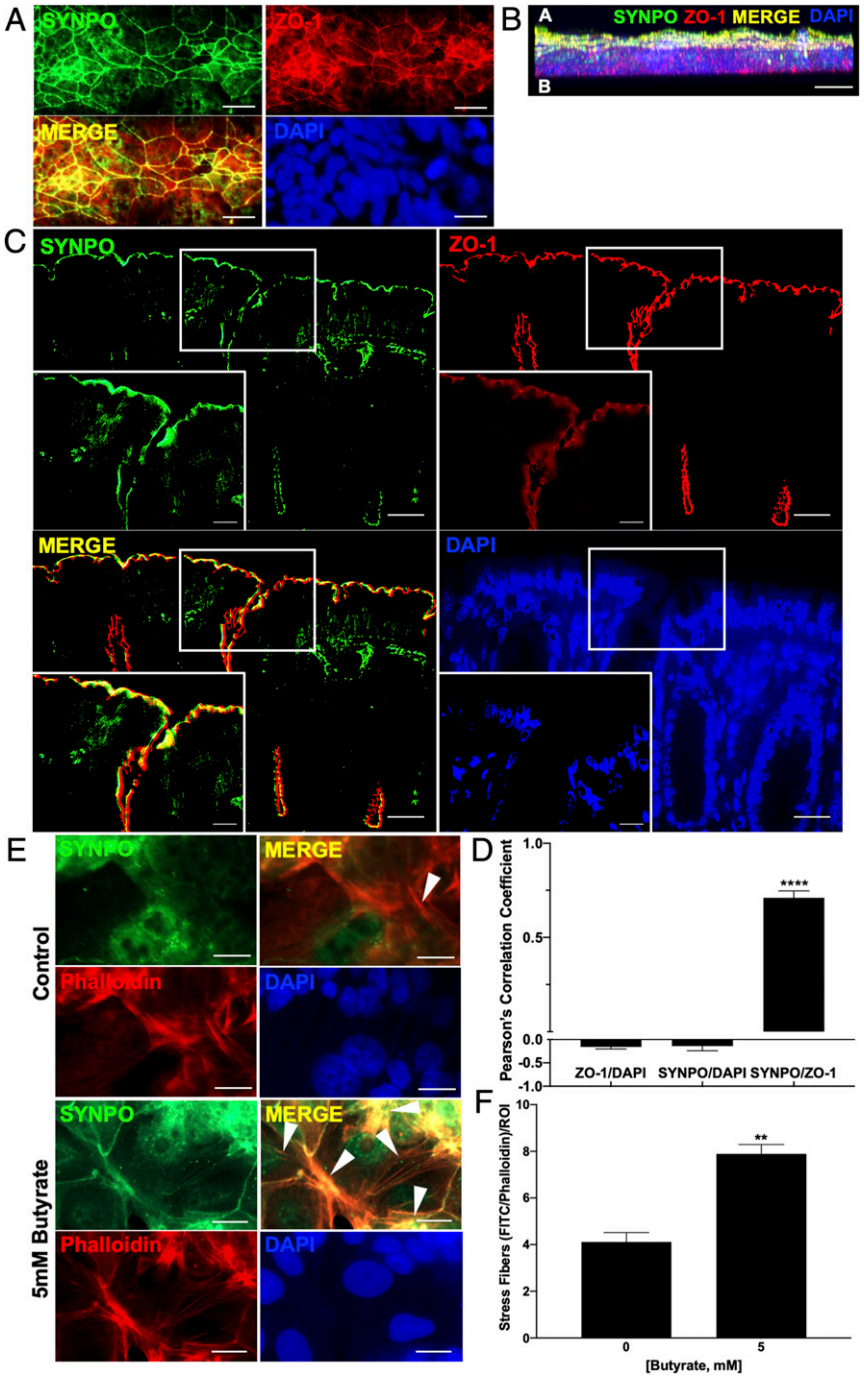

Fig. 4. Localization of SYNPO in the intestinal mucosa. (*A*) SYNPO and ZO-1 fluorescent staining localized to the tight junction in T84 cells. (Scale bar: 20 μm, 400×.) (*B*) Confocal *z* axis image of apical localization of SYNPO and ZO-1 and basolateral localization of the nuclear DAPI stain. (Scale bar: 10 μm, 1000×.) (*C*) SYNPO and ZO-1 localization to the tight junction in mouse colonic tissue. (Scale bar: 20 μm, 400×; *Inset*: 10 μm, 1,000×.) (*D*) PCC for colocalization of SYNPO to ZO-1 (SYNPO/ZO-1), SYNPO to DAPI (SYNPO/DAPI), and ZO-1 to DAPI (ZO-1/DAPI). PCC range from −1 (exclusion of pixels) to 1 (complete overlap of pixels, n = 4–5; error bars: SEM, $^{****}P < 0.0001$ by one-way ANOVA, Fisher's multiple comparisons). (*E*) SYNPO and phalloidin/actin fluorescent staining in T84 cells. White arrowhead, stress fiber localization. (Scale bar: 20 μm, 400×.) (*F*) Quantification of number of phalloidin actin stress fibers colocalized with SYNPO per ROI at 400× (n = 5; error bars: SEM, $^{**}P < 0.01$ by Student's t test).

SYNPO Is Regulated by Microbiota-Derived Butyrate and Altered by Colitic Disease In Vivo. C57BL/6 mice were treated with a combination of antibiotics to deplete their microbiota (*SI Appendix*, Fig. S4) and then replenished with tributyrin, a butyrate prodrug, to determine the role of butyrate in regulating SYNPO in vivo. Relative to control (CNTL) mice, antibiotics-treated microbiota-depleted (ABX) mice showed a significant decrease in SYNPO protein ($P < 0.05$), which was reversed with tributyrin oral gavage (ABX + TB) (Fig. 6 *A* and *B*). Additionally, C57BL/6 germfree (GF) mice exhibited decreased IEC SYNPO protein expression compared to C57BL/6 wild-type (WT) mice, and GF mice given tributyrin also demonstrated a significant increase in SYNPO (Fig. 6 *C* and *D* and *SI Appendix*, Fig. S5). We also surveyed the ileum and jejunum of WT mice in comparison to the colon,

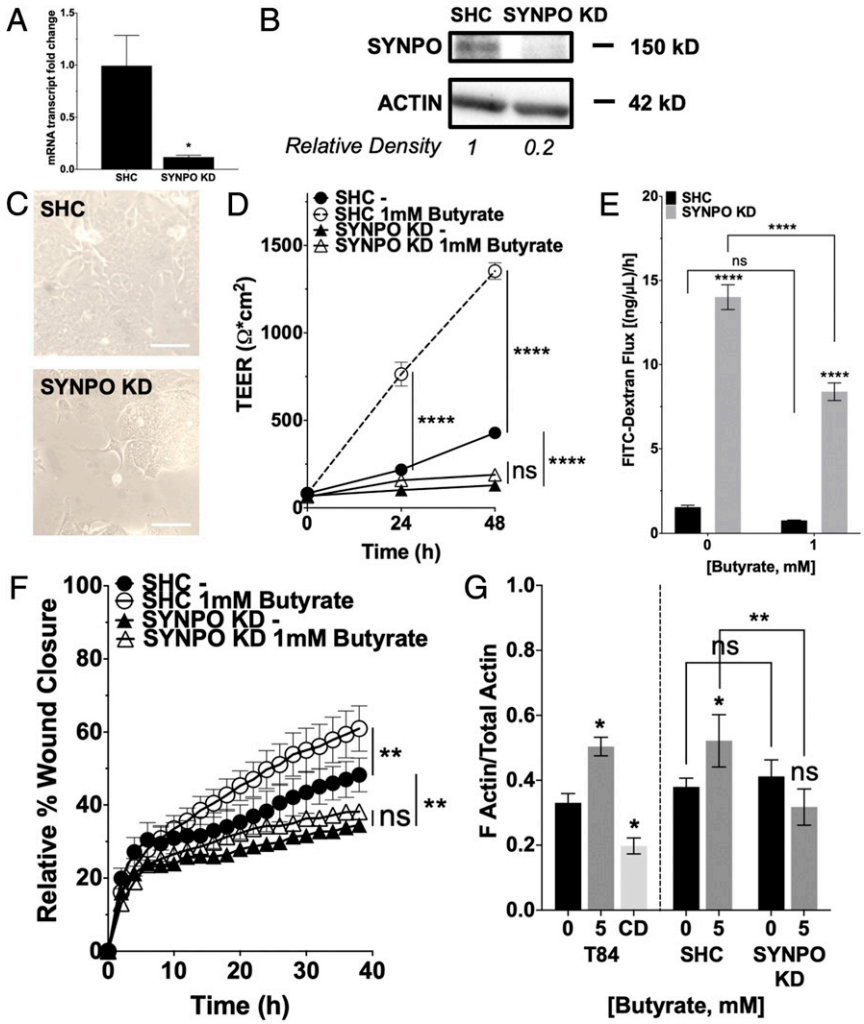

Fig. 5. Role of SYNPO in barrier function and wound healing. (*A*) *SYNPO* mRNA expression in SHC and KD cells ($n = 3$; error bars: SEM, $^{*}P < 0.05$ by Student's *t* test). (*B*) SYNPO protein expression in SHC and SYNPO KD cells and densitometry. (*C*) Bright-field microscopy images of SHC and SYNPO KD cells. (Scale bar: 100 μm, 200×.) (*D*) TEER measurements over time in SHC and KD cells treated with 1 mM butyrate ($n = 6$; error bars: SEM, $^{****}P < 0.0001$ by two-way ANOVA, Fisher's multiple comparison). (*E*) Cell layer permeability flux rate assay using 3-kDa FITC-dextran in SHC and KD cells treated with 1 mM butyrate ($n = 6$; error bars: SEM, $^{****}P < 0.0001$ by two-way ANOVA, Fisher's multiple comparison). (*F*) Scratch wound healing monitored over time by relative wound closure percentage in SHC and KD cells treated with 1 mM butyrate ($n = 5$; error bars: SEM, $^{**}P < 0.01$ by two-way ANOVA, Fisher's multiple comparison). (*G*) Ratio of F-actin to total actin in T84 cells treated with 5 mM butyrate or 10 μM cytochalasin D, and SHC and SYNPO KD cells treated with 5 mM butyrate ($n = 6$; error bars: SEM, $^{*}P < 0.05$, $^{**}P < 0.01$ by 1-way ANOVA, Fisher's multiple comparison).

which has the highest concentrations of butyrate, and found that the ileum and jejunum have significantly less expression of SYNPO, as quantified by relative immunofluorescence intensity normalized to ZO-1 (*SI Appendix*, Fig. S6). When 129S1 mice were subjected to dextran sulfate sodium (DSS) colitis, DSS significantly decreased SYNPO protein compared to water control (H_2O, $P < 0.0001$) (Fig. 6 *E* and *F*). DSS mouse colonic tissue showed intact ZO-1 staining but a significant decrease in SYNPO staining compared to control (*SI Appendix*, Fig. S7). In the DSS mice, colonic tissues with active disease marked by inflammatory infiltration and crypt and epithelial damage and no disease both showed decreased SYNPO staining but intact ZO-1 (*SI Appendix*, Fig. S7 *B* and *C*). Western blot confirmed that ZO-1 protein levels did not change with DSS colitis (*SI Appendix*, Fig. S8). Correspondingly, T84 cells treated with cytomix, a mixture of proinflammatory cytokines (10 ng/mL each of TNF-α, IL-1β, and IFN-γ) showed a significant decrease in *SYNPO* mRNA compared to control cells ($P < 0.01$, Fig. 6*G*), suggesting that inflammation negatively impacts SYNPO expression.

SYNPO Is Critical to Maintaining Intestinal Homeostasis in Health and Mucosal Disease. Whole body *Synpo*$^{-/-}$ 129S1 mice (confirmed by genotyping, Western blot, and immunofluorescence in mouse colonic tissue) (Fig. 7*A* and *SI Appendix*, Fig. S9) were utilized to define the contribution of SYNPO to intestinal disease in vivo. Based on histologic analysis, no significant colonic pathologies were noted in *Synpo*$^{-/-}$ mice at baseline.

WT and *Synpo*$^{-/-}$ (knockout [KO]) mice were subjected to 3% DSS or water control for 5 d, recovered for 5 d, and then killed on day 10. Throughout the DSS cycle, we monitored disease activity index (DAI) encompassing body weight, stool consistency, and bleeding. *Synpo*$^{-/-}$ mice showed enhanced susceptibility to DSS colitis compared to WT mice, exhibiting significantly higher DAI scores at days 7 to 10 ($P < 0.0001$). *Synpo*$^{-/-}$ mice revealed symptoms of disease at earlier time points and did not recover whereas the WT showed a lower magnitude of disease with rapid recovery after day 7 (Fig. 7*B*). Upon killing, *Synpo*$^{-/-}$ mice showed a significantly shorter colon than their WT counterparts ($P < 0.05$, Fig. 7*C*).

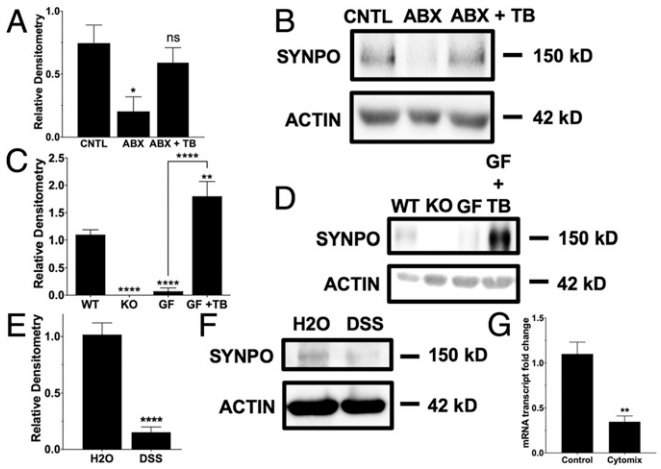

Fig. 6. Impact of the microbiota and colitic disease on SYNPO. (*A*) Whole tissue SYNPO protein expression in control (CNTL), antibiotics-treated microbiota-depleted (ABX), and tributyrin add-back mice (ABX + TB) (n = 4–5; error bars: SEM, $*P < 0.05$ by one-way ANOVA, Fisher's multiple comparison). (*B*) Representative Western blot for CNTL, ABX, and ABX + TB mice. (*C*) SYNPO protein expression in epithelial scrapings of WT, SYNPO KO (negative control), GF, and GF and tributyrin (GF + TB) mice (n = 4–5; error bars: SEM, $**P < 0.01$, $****P < 0.0001$ by one-way ANOVA, Fisher's multiple comparison). (*D*) Representative Western blot for WT, GF, and GF + TB mice. (*E*) Whole tissue SYNPO protein expression in control (H_2O) mice and mice subjected to DSS colitis (n = 5–6; error bars: SEM, $****P < 0.0001$ by Student's t test). (*F*) Representative Western blot for H_2O and DSS mice. (*G*) *SYNPO* mRNA expression in T84 cells treated with cytomix for 6 h (n = 6; error bars: SEM, $**P < 0.01$ by Student's t test).

Intestinal barrier integrity was assessed at the end of the study utilizing 70-kDa FITC-dextran oral gavages, which showed that, at baseline, the *Synpo*$^{-/-}$ mice harbored a baseline barrier defect (KO: 77.28 ± 15.190 μg/mL; to WT: 17.95 ± 4.907 μg/mL, $P < 0.01$). This barrier defect was further enhanced in colitic animals (KO DSS: 142.00 ± 23.280 μg/mL; to WT DSS: 69.39 ± 6.710 μg/mL, $P < 0.01$) (Fig. 7*D*). Tissue damage associated with colitis was assessed histologically. As shown in Fig. 7*E*, histologic scores reflecting inflammatory infiltration and epithelial damage revealed significantly enhanced damage in *Synpo*$^{-/-}$ mice compared to WT mice ($P < 0.001$). Representative images shown in Fig. 7*F* demonstrate a complete loss of crypt morphology due to inflammatory infiltration that led to severe epithelial damage in *Synpo*$^{-/-}$ mice. WT DSS mice displayed a subdued level of inflammatory infiltration with moderate epithelial and crypt damage. Overall, the loss of SYNPO impeded intestinal barrier function and exacerbated colitic disease. We also found that DSS treatment significantly decreased cecal butyrate content in both WT and *Synpo*$^{-/-}$ mice (*SI Appendix*, Fig. S10*A*).

Lastly, we supplemented WT and *Synpo*$^{-/-}$ mice with 5 mM butyrate in their drinking water during DSS to determine if butyrate regulation of SYNPO contributed to intestinal homeostasis. While the therapeutic influence of butyrate supplementation was subtle in WT mice over the course of the experiment, it was abundantly clear that butyrate supplementation did not significantly improve disease activity in *Synpo*$^{-/-}$ mice. For example, butyrate significantly decreased disease activity by day 6 in WT animals whereas the *Synpo*$^{-/-}$ mice given butyrate showed no significant difference in DAI compared to their no-butyrate controls (*SI Appendix*, Fig. S10*C*). Day 6 also corresponded to the peak rectal bleeding where WT mice given butyrate showed no signs of bleeding compared to WT mice without butyrate, whereas *Synpo*$^{-/-}$ mice had similar bleeding scores between butyrate and control (*SI Appendix*, Fig. S10*D*). Notably, at time of killing, WT mice given butyrate showed significantly lower histological scores compared to no-butyrate controls whereas *Synpo*$^{-/-}$ mice had higher, similar histological scores regardless of butyrate supplementation (Fig. 7*G* and *SI Appendix*, Fig. S10*E*). Importantly, intestinal barrier permeability as assayed through FITC-dextran flux showed a similar pattern, with a significant decrease indicative of improved barrier function seen in WT mice given butyrate, whereas the barrier improvement was lost in *Synpo*$^{-/-}$ mice (Fig. 7*H*). Taken together, these studies implicate a role for butyrate-induced SYNPO in intestinal barrier and wound healing in vivo.

Discussion

An understanding of the mechanisms through which the host communicates to and from the microbiota is an area of significant interest (32). Given the high density of microbes in the colon, epithelial cells are anatomically positioned to function as the primary sensor for host–microbial communication. We report here that the SCFA butyrate selectively regulates epithelial permeability and mucosal wound healing through SYNPO-dependent mechanisms.

SCFAs produced by the intestinal microbiota exhibit differential utilization and specialized influence dependent on location. For example, butyrate is primarily sequestered to the intestine and is used by the colonocytes as a readily available energy source while acetate and propionate enter hepatic circulation in significant quantities. Propionate is primarily processed and used by the liver for gluconeogenesis whereas acetate reaches peripheral circulation as precursors for lipogenesis and is metabolized by the brain and cardiac/skeletal muscle (33–35). Functioning as a selective barrier and undergoing constant and rapid turnover, IECs are highly energetically demanding (36). Cell migration and tight junction formation are crucial to an intact barrier and require actin cytoskeletal rearrangements that are energetically demanding, consuming nearly 20% of all high energy phosphates (31). Our work here demonstrates that, in addition to energy provision, butyrate acts locally and uniquely in the intestinal mucosa to regulate gene expression for barrier formation and wound restitution to sustain homeostasis. This response was not observed with acetate or propionate. Unbiased profiling of butyrate-exposed cells identified a cluster of actin-associated proteins with the potential to regulate barrier and wound healing. Among these targets, we identify an intestinal epithelial tight junction protein, SYNPO, that is directly regulated by butyrate through HDAC inhibition. Butyrate is a well-established HDAC inhibitor, which is unique among SCFAs. Propionate shows significantly reduced HDAC inhibition capacity, and acetate carries effectively no HDAC inhibition ability (37). Thus, in addition to functioning as an evolved energy source in the mucosa, butyrate effectively coordinates the compartmentalized control of barrier function through selective regulation of actin-associated genes.

Original studies described SYNPO in the foot processes of renal podocytes and the postsynaptic densities and dendritic spines of telencephalic neurons as a cell shape and motility regulator. Through binding F-actin, SYNPO coordinates the cell cytoskeleton, especially the localization of actin to the tight junction (38). The perijunctional cytoskeleton features an extensive network of F-actin bundles connected to the tight junction to form a barrier to regulate paracellular passage and a dense circumferential actomyosin ring connected through adhesion proteins of the adherens junction to form a dynamic contractile apparatus to mediate cell–cell contact (39). SYNPO not only regulates the expression of α–actinin-4 (ACTN4), an actomyosin ring-associated protein critical to cell contractility, but also facilitates ACTN4 accumulation at the adherens junction (40). Our work demonstrates that butyrate may also induce ACTN4 expression, suggesting that butyrate influences both the tight junction and the adherens junction protein expression, and that butyrate-mediated SYNPO induction may concomitantly

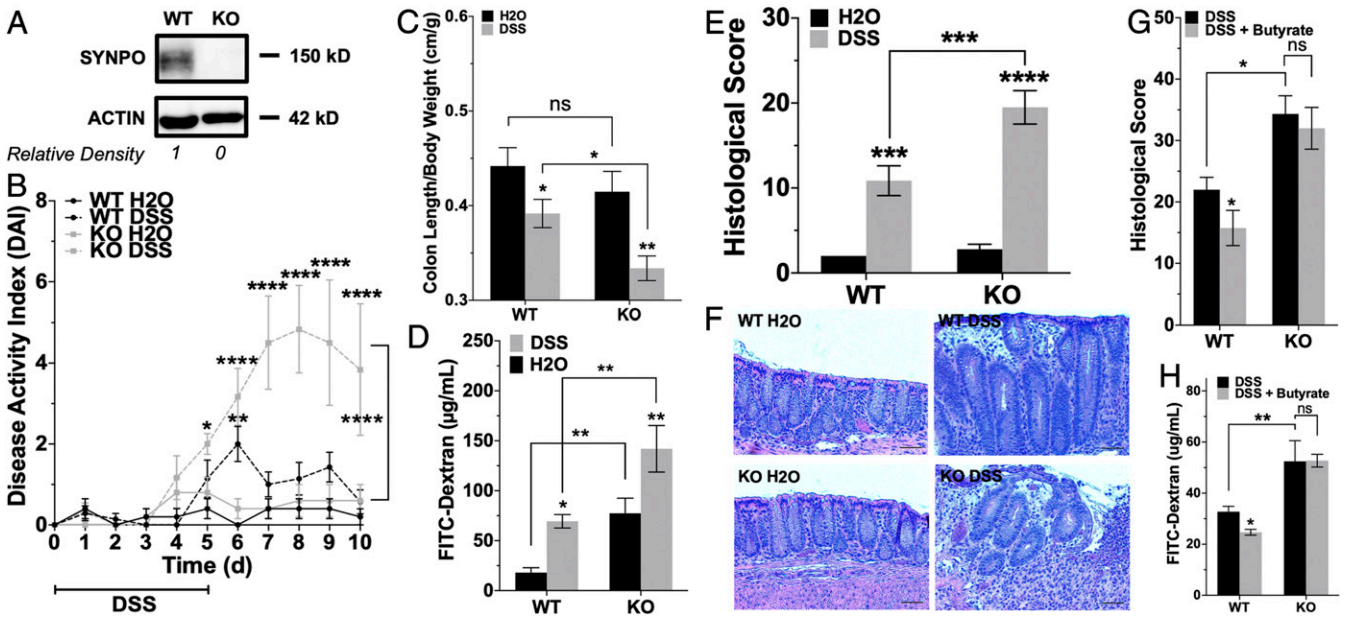

Fig. 7. Importance of SYNPO to intestinal homeostasis and mucosal disease. (*A*) SYNPO protein expression in WT and SYNPO KO mice and densitometry. (*B*) DAI scores of WT and KO mice subjected to DSS versus H_2O, maximum DAI 12 ($n = 5$–6; error bars: SEM, $^*P < 0.05$, $^{**}P < 0.01$, $^{****}P < 0.0001$ by two-way ANOVA, Fisher's multiple comparison). (*C*) Colon length to body mass ratios of WT and KO mice subjected to DSS versus H_2O ($n = 5$–6; error bars: SEM, $^*P < 0.05$, $^{**}P < 0.01$ by two-way ANOVA, Fisher's multiple comparison). (*D*) Combined serum and urine FITC-dextran in WT and KO mice subjected to DSS versus H_2O ($n = 5$; error bars: SEM, $^*P < 0.05$, $^{**}P < 0.01$ by two-way ANOVA, Fisher's multiple comparison). (*E*) Histological scoring of colon tissue of WT and KO mice subjected to DSS versus H_2O, maximum histological score 40 ($n = 5$–6; error bars: SEM, $^{***}P < 0.001$, $^{****}P < 0.0001$ by two-way ANOVA, Fisher's multiple comparison). (*F*) Representative histology images of the extent of damage in colon tissue of WT and KO mice subjected to DSS versus H_2O. (*G*) Histological scoring of colon tissue of WT and KO mice subjected to DSS with or without butyrate supplementation ($n = 5$; error bars: SEM, $^*P < 0.05$ by two-way ANOVA, Fisher's multiple comparison). (*H*) Combined serum and urine FITC-dextran in WT and KO mice subjected to DSS with or without butyrate supplementation ($n = 5$; error bars: SEM, $^*P < 0.05$, $^{**}P < 0.01$ by two-way ANOVA, Fisher's multiple comparison).

increase binding partner ACTN4 for overall IEC function. Loss of SYNPO in podocyte results in increased barrier permeability and loss of stress fibers that impaired cell migration (41). Consistent with the characterizations in the kidneys and the brain, we establish here that SYNPO is an essential tight junction protein of the intestinal mucosa, required for barrier formation and wound restitution. SYNPO localizes to the tight junction in IECs for barrier modulation while also coordinating stress fibers for cell migration. Loss-of-function studies revealed that SYNPO is a necessary aspect of butyrate regulation of barrier promotion and wound closure. The actin cytoskeletal network and affiliated proteins are tightly regulated to maintain and restore homeostasis, and SYNPO is a key microbiota-regulated protein involved in this intestinal system.

During bouts of mucosal inflammation, such as that seen in IBD, intestinal homeostasis is perturbed, and the intestinal epithelium incurs repeated bouts of damage. Such a loss of homeostasis is due in part to the well-established dysbiosis seen in IBD where butyrate-producing microbiota are selectively depleted. Our studies here suggest that another integral aspect is butyrate-regulated expression of actin-associated proteins, including SYNPO. Chronic systemic inflammation reduces SYNPO expression in neurons (42), and we observe here that *SYNPO* mRNA decreases when T84 cells are treated with a mix of proinflammatory cytokines termed "cytomix" that is known to diminish barrier function (43). TNF-α has been shown to increase SYNPO protein degradation (44), and we find that mice subjected to DSS colitis also show a significant decrease in SYNPO protein expression, indicative that SYNPO is disrupted during inflammation, and the loss of SYNPO results in disturbed homeostasis. Interestingly, this is not due simply to the loss of the epithelium from the noxious influence of DSS as areas where ZO-1 remained intact revealed a loss of SYNPO. In patients with glomerulonephritis, increased serum creatinine indicative of disease progression correlated with increased urine secretion of SYNPO from the kidneys (45). Possible secretion of SYNPO in a diseased colon may be an explanation of the loss seen, which would worsen disease progression but could possibly become a fecal biomarker of colitic disease. The DSS colitis model also selectively depletes butyrate content over other SCFAs in the colon, which mirrors butyrate deficiency seen in IBD (46). Consistent with these previous studies, we find that cecal butyrate levels are decreased during DSS, and the decreased level of butyrate could lead to decreased SYNPO expression. These data together suggest that mucosal inflammation directly reduces both butyrate and SYNPO, with further indirect loss of SYNPO through diminished butyrate-producing microbiota. We highlight the direct regulation of butyrate on SYNPO in vivo such that antibiotic elimination of the microbiota abolishes SYNPO expression that is rescued by butyrate supplementation.

Our studies in *Synpo*$^{-/-}$ mice characterize an intestinal phenotype. While no morphological differences were evident, *Synpo*$^{-/-}$ animals showed a notable increase in intestinal permeability at baseline. The importance of SYNPO became magnified in the context of mucosal inflammation. Previous work showed that these mice displayed slight neurological deficiency, with impaired activity-dependent long-term synaptic plasticity due to lack of functional dendritic spine apparatuses, but no other physiological deficits. Ultrastructural analysis of podocytes in *Synpo*$^{-/-}$ mice appeared normal until the kidneys were subjected to lipopolysaccharide (LPS)-induced glomerular damage and resultant nephrotic syndrome, or protamine sulfate-induced podocyte foot process effacement, both to which the mice exhibited increased susceptibility and impaired recovery (47). Likewise, upon submitting *Synpo*$^{-/-}$ mice to DSS colitis, which essentially effaces the intestinal epithelial monolayer by damaging the IECs, a similar

pattern to the kidney injury induced by protamine sulfate was revealed as DSS elicited significantly worse disease as a result of SYNPO loss. Correspondingly, SYNPO dysregulation and ensuing barrier and motility dysfunction are apparent in another inflammatory mucosal disease, eosinophilic esophagitis (48). Furthermore, genome-wide association studies of IBD and Crohn's disease show possible significant single nucleotide polymorphisms in the genomic region of SYNPO (49, 50), and microarray analysis has demonstrated differential expression of SYNPO2 (also called myopodin), a SYNPO homolog (51), in patients with ulcerative colitis (52). Our data suggest that SYNPO is critical in preventing disease and promoting recovery in the GI tract.

Some aspects of disease activity in DSS colitis were improved by butyrate supplementation in WT mice, and it is notable that no such protection was afforded in *Synpo*$^{-/-}$ mice. Demonstrating overall colitic disease prevention/protection with butyrate supplementation during DSS has not been definitively achieved with consistent results across studies, but, when specific metrics such as cytokine expression and bleeding scores have been quantified, those have revealed the significant influence of butyrate (53–55). Similarly, in our studies, we observed butyrate supplementation to significantly decrease intestinal permeability in WT mice subjected to DSS, but this promotion of barrier function was lost in *Synpo*$^{-/-}$ mice subjected to DSS and given butyrate. This shows a key physiological role for butyrate regulation of SYNPO in regulating intestinal barrier function, especially as we have identified SYNPO as a critical intestinal tight junction protein. Histological scores also improved in butyrate-supplemented WT mice, with these mice showing more intact crypt structure compared to control, whereas *Synpo*$^{-/-}$ mice with or without butyrate exhibited significantly higher histological scores with absolute loss of crypt structure. Bleeding scores also improved in WT mice given butyrate, but not in *Synpo*$^{-/-}$ mice. Taken together, these results provide a role for butyrate in wound healing. As butyrate regulation of the intestinal mucosa is multifaceted and can influence not only the epithelial cells but also immune cells, our results contribute to an evolving role for SCFAs in mucosal homeostasis. The characterization of SYNPO as an IEC tight junction protein that is specifically regulated by microbiota-derived SCFA butyrate thus continues its therapeutic potential and furthers our understanding of the fine-tuned relationship between the host and microbes.

Materials and Methods

For details, please refer to *SI Appendix, Supplemental Materials and Methods*.

Antibiotic Microbiota Depletion and Tributyrin Supplementation. Eight-week-old female C57BL/6 mice were preadministered an antibiotic mixture consisting of 1 mg/mL ampicillin, gentamicin, and neomycin, and 0.5 mg/mL metronidazole and vancomycin (Sigma-Aldrich) for 5 d ad libitum. Then, a 200-μL bolus of oral tributyrin gavage supplementation (Sigma-Aldrich) was given daily for 3 d.

TEER Measurement. Cells were plated on 0.33-cm^2 transwell inserts (0.4 μm; Corning) at 58,000 cells per insert, and TEER readings were measured over 48 h using an epithelial volt-ohm meter (EVOM^2, World Precision Instruments). Where indicated, the cells were treated with butyrate, propionate, or acetate.

Data Availability Statement. All data discussed in this paper are provided within the main text and tables, including supplemental material.

ACKNOWLEDGMENTS. This work was supported by NIH Grants DK1047893, DK50189, DK095491, and DK103712, and by Veterans Administration Merit Award BX002182. R.X.W. was supported by NIH National Research Service Award (NRSA) Fellowship F30DK120072 and NIH Medical Scientist Training Program Training Grant T32GM008497. J.S.L. was supported by NIH NRSA Fellowship F32DK122741. We thank Michelle Randolph (Protein Production Shared Resource Core) for help with the IncuCyte live-cell imaging system that was supported by NIH Cancer Center Support Grant P30CA046934; Dan Koyanagi and Terrin Manes for tissue sample processing, sectioning, and hematoxylin and eosin staining; Cassandra Levins (Gnotobiotic Core, Anschutz Medical Campus) for assistance with germfree mice experiments; and Timothy Wang for conducting revision experiments and data analysis.

1. L. W. Peterson, D. Artis, Intestinal epithelial cells: Regulators of barrier function and immune homeostasis. *Nat. Rev. Immunol.* **14**, 141–153 (2014).
2. J. Landy *et al.*, Tight junctions in inflammatory bowel diseases and inflammatory bowel disease associated colorectal cancer. *World J. Gastroenterol.* **22**, 3117–3126 (2016).
3. M. G. Laukoetter, P. Nava, A. Nusrat, Role of the intestinal barrier in inflammatory bowel disease. *World J. Gastroenterol.* **14**, 401–407 (2008).
4. M. A. Odenwald, J. R. Turner, Intestinal permeability defects: Is it time to treat? *Clin. Gastroenterol. Hepatol.* **11**, 1075–1083 (2013).
5. M. Iizuka, S. Konno, Wound healing of intestinal epithelial cells. *World J. Gastroenterol.* **17**, 2161–2171 (2011).
6. A. Sturm, A. U. Dignass, Epithelial restitution and wound healing in inflammatory bowel disease. *World J. Gastroenterol.* **14**, 348–353 (2008).
7. C. A. Lozupone, J. I. Stombaugh, J. I. Gordon, J. K. Jansson, R. Knight, Diversity, stability and resilience of the human gut microbiota. *Nature* **489**, 220–230 (2012).
8. G. den Besten *et al.*, The role of short-chain fatty acids in the interplay between diet, gut microbiota, and host energy metabolism. *J. Lipid Res.* **54**, 2325–2340 (2013).
9. D. R. Donohoe *et al.*, The microbiome and butyrate regulate energy metabolism and autophagy in the mammalian colon. *Cell Metab.* **13**, 517–526 (2011).
10. K. Daly, S. P. Shirazi-Beechey, Microarray analysis of butyrate regulated genes in colonic epithelial cells. *DNA Cell Biol.* **25**, 49–62 (2006).
11. C. J. Kelly *et al.*, Crosstalk between microbiota-derived short-chain fatty acids and intestinal epithelial HIF augments tissue barrier function. *Cell Host Microbe* **17**, 662–671 (2015).
12. B. T. Layden, A. R. Angueira, M. Brodsky, V. Durai, W. L. Lowe Jr., Short chain fatty acids and their receptors: New metabolic targets. *Transl. Res.* **161**, 131–140 (2013).
13. J. R. Davie, Inhibition of histone deacetylase activity by butyrate. *J. Nutr.* **133** (suppl. 7), 2485S–2493S (2003).
14. R. Thibault *et al.*, Butyrate utilization by the colonic mucosa in inflammatory bowel diseases: A transport deficiency. *Inflamm. Bowel Dis.* **16**, 684–695 (2010).
15. W. Babidge, S. Millard, W. Roediger, Sulfides impair short chain fatty acid beta-oxidation at acyl-CoA dehydrogenase level in colonocytes: Implications for ulcerative colitis. *Mol. Cell. Biochem.* **181**, 117–124 (1998).
16. H. Liu *et al.*, Butyrate: A double-edged sword for health? *Adv. Nutr.* **9**, 21–29 (2018).
17. H. M. Hamer *et al.*, Review article: The role of butyrate on colonic function. *Aliment. Pharmacol. Ther.* **27**, 104–119 (2008).
18. P. Mundel *et al.*, Synaptopodin: An actin-associated protein in telencephalic dendrites and renal podocytes. *J. Cell Biol.* **139**, 193–204 (1997).
19. P. Mundel, P. Gilbert, W. Kriz, Podocytes in glomerulus of rat kidney express a characteristic 44 KD protein. *J. Histochem. Cytochem.* **39**, 1047–1056 (1991).
20. N. Kannan, V. W. Tang, Synaptopodin couples epithelial contractility to α-actinin-4-dependent junction maturation. *J. Cell Biol.* **211**, 407–434 (2015).
21. G. I. Mun, S. Park, J. Kremerskothen, Y. C. Boo, Expression of synaptopodin in endothelial cells exposed to laminar shear stress and its role in endothelial wound healing. *FEBS Lett.* **588**, 1024–1030 (2014).
22. J. M. Chalovich, M. M. Schroeter, Synaptopodin family of natively unfolded, actin binding proteins: Physical properties and potential biological functions. *Biophys. Rev.* **2**, 181–189 (2010).
23. T. Pelaseyed, A. Bretscher, Regulation of actin-based apical structures on epithelial cells. *J. Cell Sci.* **131**, 58–65 (2018).
24. N. M. Dalesio, S. F. Barreto Ortiz, J. L. Pluznick, D. E. Berkowitz, Olfactory, taste, and photo sensory receptors in non-sensory organs: It just makes sense. *Front Physiol.* **9**, 1673 (2018).
25. S. Winans, A. Flynn, S. Malhotra, V. Balagopal, K. L. Beemon, Integration of ALV into *CTDSPL* and *CTDSPL2* genes in B-cell lymphomas promotes cell immortalization, migration and survival. *Oncotarget* **8**, 57302–57315 (2017).
26. V. Garcia-Hernandez, M. Quiros, A. Nusrat, Intestinal epithelial claudins: Expression and regulation in homeostasis and inflammation. *Ann. N. Y. Acad. Sci.* **1397**, 66–79 (2017).
27. A. Buckley, J. R. Turner, Cell biology of tight junction barrier regulation and mucosal disease. *Cold Spring Harb. Perspect. Biol.* **10**, 1–10 (2018).
28. T. Gryaznova *et al.*, Intersectin adaptor proteins are associated with actin-regulating protein WIP in invadopodia. *Cell. Signal.* **27**, 1499–1508 (2015).
29. D. Huszar, M. E. Theoclitou, J. Skolnik, R. Herbst, Kinesin motor proteins as targets for cancer therapy. *Cancer Metastasis Rev.* **28**, 197–208 (2009).
30. B. C. Bornhauser, C. Johansson, D. Lindholm, Functional activities and cellular localization of the ezrin, radixin, moesin (ERM) and RING zinc finger domains in MIR. *FEBS Lett.* **553**, 195–199 (2003).
31. J. S. Lee *et al.*, Hypoxanthine is a checkpoint stress metabolite in colonic epithelial energy modulation and barrier function. *J. Biol. Chem.* **293**, 6039–6051 (2018).
32. C. L. Ohland, C. Jobin, Microbial activities and intestinal homeostasis: A delicate balance between health and disease. *Cell. Mol. Gastroenterol. Hepatol.* **1**, 28–40 (2015).
33. J. H. Cummings, G. T. Macfarlane, Role of intestinal bacteria in nutrient metabolism. *JPEN J. Parenter. Enteral Nutr.* **21**, 357–365 (1997).

34. T. Nedjadi, A. W. Moran, M. A. Al-Rammahi, S. P. Shirazi-Beechey, Characterization of butyrate transport across the luminal membranes of equine large intestine. *Exp. Physiol.* **99**, 1335–1347 (2014).
35. E. Boets *et al*., Systemic availability and metabolism of colonic-derived short-chain fatty acids in healthy subjects: A stable isotope study. *J. Physiol.* **595**, 541–555 (2017).
36. S. R. Van Der Schoor *et al*., The high metabolic cost of a functional gut. *Gastroenterology* **123**, 1931–1940 (2002).
37. M. Waldecker, T. Kautenburger, H. Daumann, C. Busch, D. Schrenk, Inhibition of histone-deacetylase activity by short-chain fatty acids and some polyphenol metabolites formed in the colon. *J. Nutr. Biochem.* **19**, 587–593 (2008).
38. J. Kremerskothen, C. Plaas, S. Kindler, M. Frotscher, A. Barnekow, Synaptopodin, a molecule involved in the formation of the dendritic spine apparatus, is a dual actin/alpha-actinin binding protein. *J. Neurochem.* **92**, 597–606 (2005).
39. A. X. Cartagena-Rivera, C. M. Van Itallie, J. M. Anderson, R. S. Chadwick, Apical surface supracellular mechanical properties in polarized epithelium using noninvasive acoustic force spectroscopy. *Nat. Commun.* **8**, 1030 (2017).
40. K. M. Patrie, A. J. Drescher, A. Welihinda, P. Mundel, B. Margolis, Interaction of two actin-binding proteins, synaptopodin and alpha-actinin-4, with the tight junction protein MAGI-1. *J. Biol. Chem.* **277**, 30183–30190 (2002).
41. K. Asanuma *et al*., Synaptopodin orchestrates actin organization and cell motility via regulation of RhoA signalling. *Nat. Cell Biol.* **8**, 485–491 (2006).
42. A. Strehl *et al*., Systemic inflammation is associated with a reduction in Synaptopodin expression in the mouse hippocampus. *Exp. Neurol.* **261**, 230–235 (2014).
43. S. F. Ehrentraut *et al*., Perturbation of neddylation-dependent NF-κB responses in the intestinal epithelium drives apoptosis and inhibits resolution of mucosal inflammation. *Mol. Biol. Cell*, mbc.E16-05-0273 (2016).
44. X. Zhang *et al*., Resolvin D1 protects podocytes in adriamycin-induced nephropathy through modulation of 14-3-3β acetylation. *PLoS One* **8**, e67471 (2013).
45. S. K. Kwon, S. J. Kim, H. Y. Kim, Urine synaptopodin excretion is an important marker of glomerular disease progression. *Korean J. Intern. Med. (Korean. Assoc. Intern. Med.)* **31**, 938–943 (2016).
46. C. J. Kelly *et al*., Oral vitamin B_{12} supplement is delivered to the distal gut, altering the corrinoid profile and selectively depleting *Bacteroides* in C57BL/6 mice. *Gut Microbes* **10**, 654–662 (2019).
47. K. Asanuma *et al*., Synaptopodin regulates the actin-bundling activity of alpha-actinin in an isoform-specific manner. *J. Clin. Invest.* **115**, 1188–1198 (2005).
48. M. Rochman, J. Travers, J. P. Abonia, J. M. Caldwell, M. E. Rothenberg, Synaptopodin is upregulated by IL-13 in eosinophilic esophagitis and regulates esophageal epithelial cell motility and barrier integrity. *JCI Insight* **2** (2017).
49. K. M. de Lange *et al*., Genome-wide association study implicates immune activation of multiple integrin genes in inflammatory bowel disease. *Nat. Genet.* **49**, 256–261 (2017).
50. A. Franke *et al*., Genome-wide meta-analysis increases to 71 the number of confirmed Crohn's disease susceptibility loci. *Nat. Genet.* **42**, 1118–1125 (2010).
51. A. Weins *et al*., Differentiation- and stress-dependent nuclear cytoplasmic redistribution of myopodin, a novel actin-bundling protein. *J. Cell Biol.* **155**, 393–404 (2001).
52. C. M. Costello *et al*., Dissection of the inflammatory bowel disease transcriptome using genome-wide cDNA microarrays. *PLoS Med.* **2**, e199 (2005).
53. P. V. Chang, L. Hao, S. Offermanns, R. Medzhitov, The microbial metabolite butyrate regulates intestinal macrophage function via histone deacetylase inhibition. *Proc. Natl. Acad. Sci. U.S.A.* **111**, 2247–2252 (2014).
54. X. Zou *et al*., Effects of sodium butyrate on intestinal health and gut microbiota composition during intestinal inflammation progression in broilers. *Poult. Sci.* **98**, 4449–4456 (2019).
55. M. Kespohl *et al*., The microbial metabolite butyrate induces expression of Th1-associated factors in $CD4^+$ T cells. *Front. Immunol.* **8**, 1036 (2017).